# An Analytical Model for Estimation of Internal Erosion Rate

S. Azadbakht[1], A. Nouri[2], D. Chan[3]

[1]*Lecturer, Department of Petroleum Systems Engineering, University of Regina, Canada*
saman.azadbakht@uregina.ca

[2]*Associate professor, Department of Civil and Environmental Engineering, University of Alberta, Canada*
anouri@ualberta.ca

[3]*Professor, Department of Civil and Environmental Engineering, University of Alberta, Canada*
dave.chan@ualberta.ca

## Abstract

Estimating erosion rate of solid particles in a porous medium is of interest to geotechnical engineers; which use analytical or numerical models for this purpose. Constitutive law of erosion is a key component in the development of such models. These models estimate the solid erosion rate as a function of various modelling parameters such as fluid velocity and time.

Using the principles of dimensional analysis, a constitutive law is proposed for assessment of the rate of erosion in relation to the fluid velocity and a dimensionless proportionality constant called the erosion coefficient, $\lambda$. Based on physics of the erosion process, experimental observations and approximation theory, $\lambda$ is expressed as a function of grain density, particle Reynolds number and porosity variation. Then, the proposed constitutive model is combined with the principle of conservation of mass to arrive at an analytical model for estimation of internal erosion rate.

The analytical model shows that the erosion rate has a nonlinear direct relationship with fluid velocity and a nonlinear inverse relationship with time. The proposed analytical model is calibrated and validated using experimental data available in the literature. The validation results show that the model estimations of erosion rate can closely reproduce experimental data.

***Keywords***: Internal erosion rate, Analytical modeling, Dimensional analysis, Approximation theory

## Introduction

Internal erosion phenomenon has been studied in different fields such as petroleum and geotechnical engineering. In internal erosion, the finer particles are transported by the seepage forces within a fixed framework formed by the coarser particles. Internal erosion is a common problem encountered in earthen structures such as water dams, river/highway embankments and coastal protection structures and it usually has detrimental effects on the stability of such structures. Generally, this form of mass transport doesn't involve direct geometrical changes in the shape of the porous media; even though particle rearrangement may happen. Other equivalent terms for internal erosion are "piping erosion" and "suffusion".

In civil engineering terminology, internal erosion is also known as "filter instability". An ideal (stable) filter allows seepage of fluids through it but at the same time, prevents the erosion of finer particles. Karl Terzaghi is believed to be the first researcher who conducted laboratory experiments to study filter instability mechanisms in the 1920's (Nguyen, 2012). Almost all of the works in the area of internal erosion modeling focus on determining the filter stability criteria which are the rules prescribing the relative percentages of fine and coarse components of the filter to eliminate or minimize internal erosion (de Graauw et al. 1984; Kenny and Lau, 1985; Skempton and Brogan, 1994).

Urban regions are among areas where the internal erosion of subsurface soil can be problematic. In some cities, aggressive water pumping from subsurface water tables, on which the cities are built, have drawn the attention to the possibility of erosion of finer portions of the subsurface soil and the consequent changes in soil's physical and mechanical properties. Researchers have shown that changes in soil's physical and mechanical properties due to internal erosion can potentially lead to surface subsidence and instability of buildings and structures (Sterpi 2003; Cividini and Gioda, 2004; Cividini et al. 2009).

The phenomenon of internal erosion in soils has been studied extensively both experimentally (Lafleur, 1984; Tomlinson and Vaid, 2000; Bendahmane et al., 2008; Richards and Reddy, 2010; Ke and Takahashi, 2014; Correia dos Santos et al., 2015; Hunter and Bowman, 2018) and numerically (Muir Wood et al., 2010; Bonelli and Marot, 2011; Zou et al., 2013; Liang et al., 2017; Yang et al., 2018). A key component in analytical and numerical models used to simulate erosion of solid particles in a porous medium is the erosion constitutive law. Constitutive laws for erosion accompany the law of conservation of mass for the solid phase. Depending on the degree of coupling between erosion, fluid flow and deformation behaviour of the porous medium, other constitutive laws may be required to address the possible interaction between these phenomena. An erosion model based on three-phase mixture theory was introduced by Vardoulakis et al. (1996). In this work, model formulation satisfies the principle of conservation of mass for solid, fluid, and fluidized solid phases along with Darcy's law and a constitutive law for mass generation in the following form:

$$\dot{m} = \rho_s \lambda (1-\varphi) c \|\bar{q}_i\| \quad \textbf{(1)}$$

This constitutive law is inspired by the experimental works of Sakthivadivel (1967). In this equation, $\dot{m}$ is the solid erosion rate, $\rho_s$ is the grain density, $\lambda$ is the erosion coefficient, $\varphi$ is the rock porosity, $c$ is the concentration of solids in the fluid phase, $\bar{q}_i$ is the flow flux of the mixture

of solids and fluid and ‖ ‖ represents the Euclidean norm of a vector. The resulting system of equations is solved assuming 1-D radial fluid flow to study internal (piping) and surface erosion phenomena by enforcing different boundary conditions.

Stavropoulou et al. (1998) used a modified constitutive law for mass generation which stops the internal erosion process when solid concentration in the fluid phase reaches a critical value:

$$\dot{m} = \rho_s \lambda (1-\varphi)(c - \frac{c^2}{c_{cr}})\|\bar{q}_i\| \quad \textbf{(2)}$$

Here, $c_{cr}$ is a critical concentration of the solids in the fluid phase at which the rates of solid erosion and deposition become equal and, thus, the net rate of erosion becomes zero.

Similar forms of the constitutive laws presented above have been used by Skjaerstein et al. (1997), Papamichos and Malmanger (1999), Yi (2001), Wang and Xue (2002), Fjaer et al. (2004), Wang et al. (2005), Servant et al. (2006), Detournay et al. (2006), Detournay (2008), Papamichos (2010), and Azadbakht et al. (2012).

Sterpi (2003) used a constitutive law for numerical modelling of internal erosion which was obtained by fitting a curve to the experimental data. This constitutive law was used in a numerical model to estimate the surface subsidence due to internal erosion of soil particles in subsurface water tables. A similar approach was used by Cividini et al. (2009).

Equations 1 and 2 are among the popular forms of constitutive laws used in the literature for numerical modeling of internal and surface erosion processes. In these equations, the erosion coefficient, $\lambda$, is a calibration parameter and thus, it has to be determined experimentally. The common practice is to assign values of $\lambda$ in a way that results a match between the numerical and experimental values of the eroded mass. The erosion coefficient, however, is not a constant and may be affected by variations in particle diameter, porosity, fluid viscosity and fluid velocity.

This paper focuses on developing an analytical model for estimation of internal erosion rate of solid particles in a porous medium. First, using principles of dimensional analysis and approximation theory, a modified constitutive law for erosion is proposed which relates the rate of erosion and fluid velocity through the erosion coefficient as a constant of proportionality. In the modified formulations, it is proposed that the erosion coefficient is a function of particle density, porosity variation and a dimensionless parameter called particle Reynolds number. Next, the modified erosion law is combined with the principle of conservation of mass to arrive at an analytical model for estimation of internal erosion rate in a porous medium.

The proposed analytical model has two calibration parameters which are expressed as functions of hydraulic gradient. A series of laboratory tests obtained from the literature are used to calibrate and validate the model. Results of model validation show a good agreement between the model predictions and the experimental erosion rates.

## Mathematical Modeling

In this section, first, the modified constitutive law for particle erosion rate in porous media is presented using the principles of dimensional analysis. Next, the formulation for calculating the critical fluid velocity is derived based on analytical relations.

**Modified Erosion Constitutive Law**

The purpose here is to determine the amount of solid mass that is eroded in a porous medium with a certain grain density, porosity, and grain size distribution, when it is subjected to a flowing fluid of certain velocity and viscosity. Generally, it can be assumed that there is a lower bound of fluid velocity which we call the "critical velocity". The erosion process is expected to start only when the fluid velocity exceeds this lower limit.

The general form of the relationship between eroded mass and the other parameters stated above can be shown in the following form:

$$m = f\left[(v_f - v_{cr}), D_p, \mu, \rho_s, (\varphi - \varphi_0), (t - t_0), V_{EB}\right] \quad \textbf{(3)}$$

where, $m$ is the *total* eroded mass, $v_f$ is the apparent (Darcy) fluid velocity, $v_{cr}$ is the apparent critical fluid velocity required to initiate the erosion process, $D_p$ is the mean diameter of the *eroded* particles, $\mu$ is the fluid dynamic viscosity, $\rho_s$ is the density of the eroded particles, $(\varphi - \varphi_0)$ is the difference between the new porosity and the initial porosity, $t_0$ is the time at which erosion starts ,$(t - t_0)$ is the time elapsed after the start of erosion process and $V_{EB}$ is volume of erosion boundary. Erosion boundary is defined as the zone in which the particles are mobilized and eroded out. In a numerical model, this could be the size of an element in the numerical mesh. In an erosion experiment, $V_{EB}$ could be considered as the volume of the test specimen. Such a zone experiences an increase in porosity as a result of the internal erosion process. Also, it should be noted that the internal erosion process is governed by the degree of uniformity of the particle assembly. In this process, finer particles are eroded and removed from the pore space formed by coarser particles. As a result, internal erosion is expected to occur only in poorly-graded assemblies of particles (assemblies with high coefficients of uniformity).

If the eroded mass is expressed as time rate and is normalized by the volume of erosion boundary, then Eq. (3) is reduced to:

$$\dot{m} = f\left[(v_f - v_{cr}), D_p, \mu, \rho_s, (\varphi - \varphi_0)\right] \quad \textbf{(4)}$$

where $\dot{m}$ is the instantaneous mass rate of eroded particles per unit volume.

The parameters in Eq. (4) have been selected based on the following criteria:

- **Dimensional requirements**: The dependent parameter in this model is the mass rate per unit volume. In order to make this parameter dimensionless, there should be parameters on the right-hand side with dimensions of mass, length, time or combinations of these dimensions. This requirement justifies the existence of $[(v_f - v_{cr}), D_p, \rho_s]$ or $[(v_f - v_{cr}), D_p, \mu]$ group of parameters on the right-hand side of this equation.
- **Physics of the problem**: Particle mobilization and erosion is due to the action of drag forces and kinetic forces of the flowing fluid. Parameters $\mu$ and $(v_f - v_{cr})$ represent these two forces, respectively.

- **Experimental and field observations**: Laboratory and field observations (Vardoulakis, 2006; Papamichos and Malmanger, 1999) show that the rate of erosion decreases with time. In other words, the larger the eroded mass, the lower the rate of erosion. Therefore, there is a relationship between the rate of erosion and the eroded mass. Since eroded mass is related to porosity changes through the law of conservation of mass, the parameter $(\varphi - \varphi_0)$ has been added to reflect this process.

By applying dimensional analysis technique, it is desirable to gain some insight into the functional form of the relationship among the parameters of Eq. (4).

There are six parameters in Eq. (4) but there are only three independent dimensions, namely; mass $[M]$, length $[L]$, and time $[T]$. An infinite number of dimensionless parameters can be formed using the parameters given in Eq. (4) but using the Buckingham's π theorem, only three of them will be independent (Hornung, 2006).

Using the parameter listed in Eq. (4), the following relations are established to represent the three standard physical measures when forming the dimensionless groups. Different combinations of these parameters can be used to form the basic standard measures but at the end, the resulting functional relationship can be reduced to the same form. Therefore, Eq. (5) through Eq. (7) are used to represent mass, length and time respectively.

$$\left[\rho_s \, D_p^3\right] = [M] \tag{5}$$

$$\left[D_p\right] = [L] \tag{6}$$

$$\left[\frac{D_p}{(v_f - v_{cr})}\right] = [T] \tag{7}$$

Using the relationships above, the parameters in Eq. (4) are non-dimensionalized one by one.

$$[\dot{m}] = [ML^{-3}T^{-1}] = \left[(\rho_s \, D_p^3)(D_p)^{-3}\left[\frac{D_p}{(v_f - v_{cr})}\right]^{-1}\right] = \left[\frac{\rho_s(v_f - v_{cr})}{D_p}\right] \tag{8}$$

$$[\mu] = [ML^{-1}\,T^{-1}] = \left[(\rho_s \, D_p^3)(D_p)^{-1}\left[\frac{D_p}{(v_f - v_{cr})}\right]^{-1}\right] = \left[\rho_s \, D_p \, (v_f - v_{cr})\right] \tag{9}$$

The third dimensionless parameter is selected to be $(\varphi - \varphi_0)$.

Using Eq. (8) and (9) and parameter $(\varphi - \varphi_0)$, Eq. (4) can be written in the following form:

$$\frac{D_p \, \dot{m}}{\rho_s \, (v_f - v_{cr})} = g\left[\frac{\rho_s \, D_p \, (v_f - v_{cr})}{\mu}, (\varphi - \varphi_0)\right] = g\left[\frac{G_s \, \rho_f \, D_p \, (v_f - v_{cr})}{\mu}, (\varphi - \varphi_0)\right] \tag{10}$$

where $g[\ ]$ denotes the function of the variables in the bracket. Using the definition of Reynolds number for a particle of diameter $D_p$ (Charlez, 1997), we have:

$$\frac{D_p\,\dot{m}}{\rho_s\,(v_f - v_{cr})} = g[G_S\,(Rp - Rp_{cr}), (\varphi - \varphi_0)] \tag{11}$$

Where, $G_s$ is the specific gravity of the particle; $Rp$ is the particle Reynolds number and $Rp_{cr}$ is the particle Reynolds number at critical fluid velocity. Eq. (11) can be further simplified into the following form:

$$\dot{m} = \frac{\lambda\,\rho_s\,(v_f - v_{cr})}{D_p} \tag{12}$$

where $\lambda$ is the erosion coefficient and is represented by the following equation:

$$\lambda = g[G_S\,(Rp - Rp_{cr}), (\varphi - \varphi_0)] \tag{13}$$

Eq. (12) can be compared to Eq. (1) and Eq. (2). It should be noted that the effect of porosity on the erosion rate is absorbed into $\lambda$ here whereas in previous works, it is explicitly stated in the form of $(1-\varphi)$. Also, $v_f$ and $\bar{q}_i$ are different notations representing the same parameter, i.e., apparent fluid velocity. We also can see that Eq. (12) has reduced a five-dimensional problem in Eq. (4) to a two-dimensional problem. As per Eq. (13), the erosion coefficient $\lambda$ is proposed to be a function of the particle specific gravity, particle Reynolds number and porosity variation.

The proposed internal erosion constitutive model, shown in Eq. (12) and Eq. (13), should satisfy the principle of conservation of mass. For an internal erosion problem, the principle of conservation of mass can be simplified into the following equation:

$$\rho_s \frac{\partial \varphi}{\partial t} = \dot{m} \tag{14}$$

Where $\dot{m}$ is the mass generation term and expresses instantaneous (tangent) erosion rate per unit volume.

**Critical Fluid Velocity**

Movement of a particle through a porous medium caused by a flowing fluid is governed by the interaction between driving forces and resisting forces. The driving forces are: 1) pressure gradient force and 2) drag force of the flowing fluid. The buoyant weight of particle can be either a driving or resisting force or it can be neutral depending on the direction of fluid flow with respect to gravity. The analytical derivation of the relationship pertaining to each one of the force components will be given below. An expression is derived based on the balance of these forces to calculate the critical fluid velocity required to initiate particle movement.

***Pressure Gradient Force***

Pressure gradient force in an arbitrary direction $n$ , $\mathrm{F}_{P,n}$, exerted on an assembly of particles with volume, *V*, is given by the following formula (Detournay et al., 2006). Here, it is assumed that $z$ is the vertical coordinate pointing upward, opposite to the direction of gravity:

$$\mathrm{F}_{P,n} = -V\,\frac{d\left(\mathrm{p} + \rho_f \mathrm{g}\, z\right)}{dn} = -V\,\frac{d\Phi}{dn} \tag{15}$$

where Φ is called fluid potential.

The volume *V* is comprised of $n_p$ particles each having a volume $V_p$. Volumes *V* and $V_p$ are related through porosity, $\varphi$. Substituting the equivalent terms in Eq. (15) yields:

$$\mathrm{F}_{P,n} = -\frac{1}{1-\varphi}\frac{d\Phi}{dn}\sum_{p=1}^{n_p} V_p \tag{16}$$

Knowing that the total pressure gradient force on volume *V* is the sum of the pressure gradient forces on individual particles each having volume $V_p$, the following relationship is used to represent the pressure gradient force on each particle in any direction $n$ :

$$\mathrm{F}_{PG,n} = -\frac{V_p}{1-\varphi}\frac{d\Phi}{dn} \tag{17}$$

***Drag Force***

Drag force of a flowing fluid in the direction $n$ exerted on an immersed body can be computed using the following equation (Charlez, 1997):

$$F_{D,n} = C_D A_{cs}\left(\frac{\rho_f {v_{A,n}}^2}{2}\right) \tag{18}$$

In Eq. (18), $C_D$ is the drag coefficient which is a function of the Reynold's number, $A_{cs}$ is the cross sectional area of the immersed body projected in the direction $n$, $\rho_f$ is fluid density and $v_{A,n}$ is the actual fluid velocity in the direction $n$. For spherical particles with diameter $D_p$ and assuming laminar fluid flow conditions, Eq. (18) reduces to the following form (Asgian et al., 1995):

$$F_{D,n} = 3\pi\,\mu\, D_p v_{A,n} \tag{19}$$

where $v_{A,n}$ is related to the component of the apparent (Darcy) velocity, $v_{f,n}$ ,through the following relationship:

$$v_{A,n} = \frac{v_{f,n}}{\varphi} = -\frac{k}{\mu\varphi}\frac{d\Phi}{dn} \quad \textbf{(20)}$$

Here, $k$ is the intrinsic permeability of the medium. Substituting Eq. (20) in Eq. (19) results in:

$$F_{D,n} = -\frac{3\pi\, D_p\, k}{\varphi}\frac{d\Phi}{dn} \quad \textbf{(21)}$$

***Gravity Force Due to Buoyant Weight of the Particle***

The gravitational force in the direction $n$ against particle movement, $F_{G,n}$, exerted on a particle with volume $V_p$ and density $\rho_s$ submerged in a flowing fluid with density $\rho_f$ is given by the following relationship:

$$F_{G,n} = (\rho_s - \rho_f) V_p\, g\, cos\, \theta_n \quad \textbf{(22)}$$

where g is acceleration due to gravity and $\theta_n$ is the angle between the direction $n$ and vertical upward direction. For vertical upward flow $\theta_n$ is zero, for horizontal flow, $\theta_n$ is 90° and for downward flow, $\theta_n$ is 180°. If fluid flow is upward, gravity resists erosion, if fluid flow is downward, gravity drives the erosion process and if fluid flow is horizontal, gravity is neutral towards the particle movement.

***Erosion Condition***

It is assumed that particles will be moved in the $n$ direction when the sum of the driving forces on the particle in that direction is larger than the resisting forces. This assumption can be expressed in the following form:

$$F_{PG,n} + F_{D,n} > F_{G,n} \quad \textbf{(23)}$$

Substituting Eq. (17), Eq. (21) and Eq. (22) in the inequality above and replacing $\frac{d\Phi}{dn}$ using Darcy's law, an expression is derived for the estimation of critical fluid velocity as follows:

$$v_{f,n} > \frac{A}{B} = v_{cr,n} \quad \textbf{(24)}$$

where parameters A and $B$ are given in Eq. (25) and Eq. (26), respectively.

$$A = (\rho_s - \rho_f) V_p\, g\, cos\, \theta_n \quad \textbf{(25)}$$

$$B = \left(\frac{V_p\, \mu}{(1-\varphi)k} + \frac{3\pi\ D_p\, \mu}{\varphi}\right) \quad \textbf{(26)}$$

Thus, in any direction, the apparent fluid velocity $v_{f,n}$ has to exceed the critical velocity, $v_{cr,n}$, given in Eq. (24) for erosion to start.

It is worth noting that Eq. (24) only sets a lower bound for the initiation of particle mobilization. Not all the particles which meet the criterion in Eq. (24) can be eroded. Some of the mobilized particles are redeposited along the way and another portion will be trapped behind pore throats that are smaller than their diameters (particle entrapment). Particle redeposition and particle entrapment are two well-known causes of diminishing erosion rates in the internal erosion process. The proposed model accounts for these processes by using a nonlinear erosion coefficient (as shown in the model calibration section of this paper).

## Sterpi (2003) Erosion Experiments

Data from a series of erosion experiments, obtained from the literature, on a well-graded silty-sand were used to calibrate and validate the proposed analytical model. Details of sample preparation and test procedures are reported in the paper by Sterpi (2003). In Sterpi (2003), the testing apparatus consisted of a permeameter in which the specimen was packed in seven layers. An upward fluid flow was induced through the specimen by applying different hydraulic gradients using an upper reservoir. Water and eroded particles were collected in a lower reservoir and the mass of eroded solids was measured at certain time intervals. Grain size distribution of the samples is shown in Figure 1 and other relevant properties are given in Table 1. Figure 2 shows the results of Sterpi (2003) erosion tests with five different hydraulic gradients. The results are reported as the percentage of eroded fines versus time. In this work, "fines" is defined as particles that pass through the standard ASTM #200 sieve (with diameter of 0.074 mm). The samples in these tests had an initial fine content of 23% by weight (Figure 1). The tests were originally conducted to estimate the amount of eroded material in subsurface water tables under various hydraulic gradients and the results were used in a numerical model to estimate subsequent surface subsidence for geotechnical assessments.

In Table 1, permeability and hydraulic conductivity are related. The difference originates from different forms of Darcy's law used in petroleum and geotechnical engineering. The relationship between these two forms of Darcy's law is given in Eq. (27):

$$v_f = \frac{k}{\mu}\frac{|\Delta\Phi|}{\Delta L} = \frac{k\gamma}{\mu}\frac{|\Delta h|}{\Delta L} = \frac{k\gamma}{\mu} i = Ki \quad \textbf{(27)}$$

where $k$ is the intrinsic permeability with unit of area, $|\Delta\Phi|$ is difference of fluid potential across sample, $\Delta L$ is sample length, $\gamma$ is unit weight of the fluid, $|\Delta h|$ hydraulic head difference across the sample, $K$ is hydraulic conductivity with unit of velocity, and $i$ is hydraulic gradient which is a dimensionless parameter.

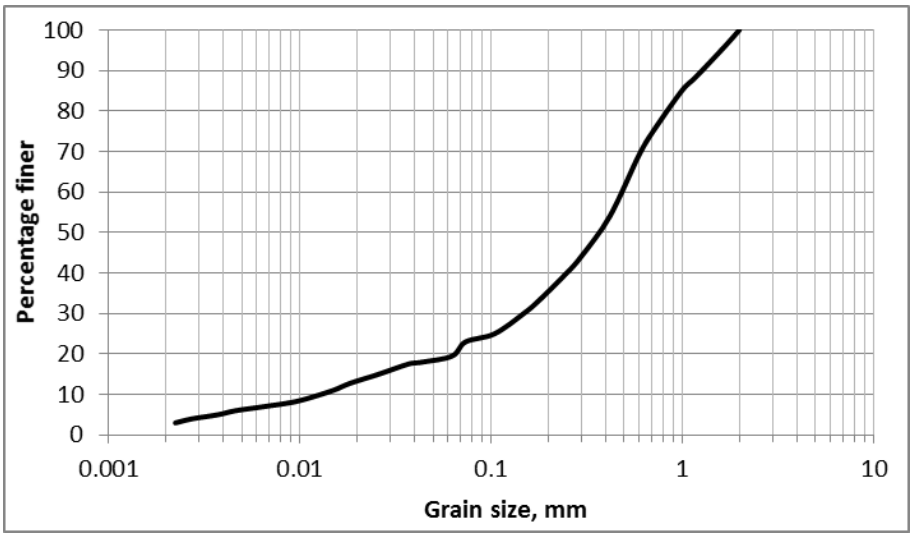


**Figure 1: Grain size distribution of the silty-sand used for laboratory experiments by Sterpi (2003) (With permission from ASCE)**

**Table 1: Properties of the silty-sand used in the experiments by Sterpi (2003)**

| Parameter | Value |
|---|---|
| **Sample diameter, m** | 0.07 |
| **Sample height, m** | 0.14 |
| **Initial porosity, $\varphi_0$** | 0.338 |
| **Specific gravity, $G_s$** | 2.72 |
| **Initial mass of test specimen, kg** | 0.97 |
| **Initial percentage of fine particles by weight, %** | 23 |
| **Hydraulic conductivity, *K*, m/sec** | 0.0001 |
| **Permeability, *k*, Darcy** | 10.33 |
| **Fluid viscosity, μ, Pa.sec** | 0.001 |

No appreciable change in permeability was reported during the testing except for Test 2 which showed an increase in permeability 5 hours after the start of the test (Figure 2). The constant permeability (with the exception of test 2) combined with the constant hydraulic gradient implies a constant fluid velocity during the testing.

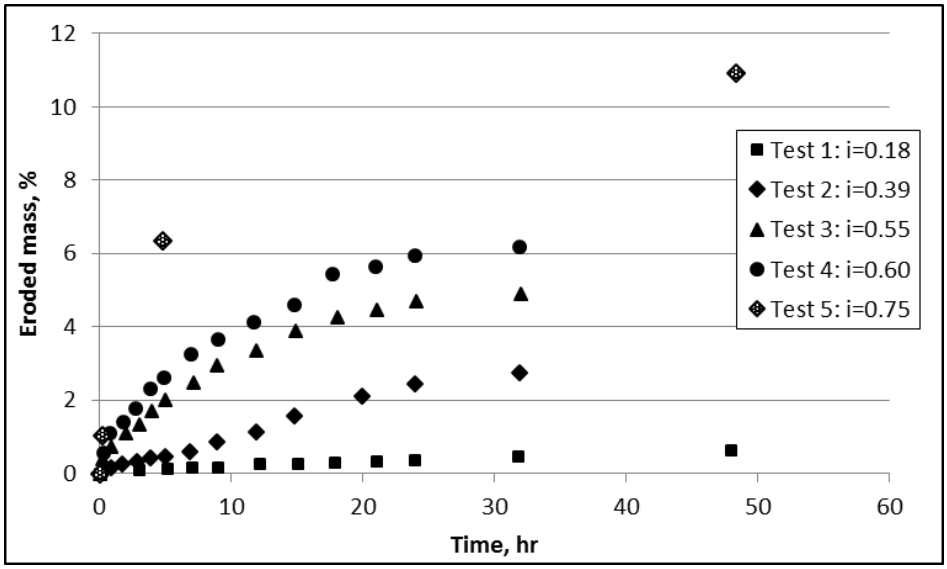


**Figure 2: Results of erosion tests by Sterpi (2003) for different hydraulic gradients (With permission from ASCE)**

## Model Calibration

The proposed modified constitutive law for internal erosion of particles in porous media is represented by Eq. (12) and Eq. (13). The purpose of this section is to offer a functional form for the erosion parameter ($\lambda$) given by Eq. (13). The actual functional form of $\lambda$ is unknown but based on experimental observations (Figure 2), we know that $\lambda$ is directly proportional to fluid velocity and inversely proportional to porosity change, $(\varphi - \varphi_0)$. In other words, a higher fluid velocity results in a higher value of $\lambda$ and higher eroded mass [higher $(\varphi - \varphi_0)$] results in a lower $\lambda$ value. Having these observations and using the approximation theory (David and Nolle, 1982), the functional from of $\lambda$ can be approximated using the following equation:

$$\lambda = \alpha \left[\frac{G_S(Rp - Rp_{cr})}{\varphi - \varphi_0}\right]^{\beta} \quad \textbf{(28)}$$

where $\alpha$ and $\beta$ are dimensionless calibration parameters.

By defining $\omega$ as:

$$\omega = \frac{G_S(Rp - Rp_{cr})}{\varphi - \varphi_0} \quad \textbf{(29)}$$

Eq. (28) can be simplified as:

$$\lambda = \alpha\, \omega^{\beta} \tag{30}$$

By taking the natural log of both sides of Eq. (30), the following equation is obtained:

$$ln\, \lambda = ln\, \alpha + \beta\, ln\, \omega \tag{31}$$

Therefore, if $ln\, \lambda$ is plotted versus $ln\, \omega$, $ln\, \alpha$ will be the intercept and $\beta$ will be the slope of the line. Experimental data given in Figure 2 are used to estimate the values of $\alpha$ and $\beta$ for each test. Using the data in Table 1 and eroded mass for each gradient given in Figure 2, the mass of eroded particles (silt and clay), $m$, can be calculated at any time for all tests, using the following formula:

$$m = p\, p_{if}\, m_t \tag{32}$$

where $p$ is the percentage of eroded fine particles (obtained from Figure 2), $p_{if}$ is the initial percentage of fine particles (obtained from Table 1) and $m_t$ is the total mass of the test specimen (obtained from Table 1).

Next, the eroded mass is normalized by the volume of the test specimen (which is the same for all tests) and is plotted as a function of time.

The values of $\dot{m}$ for each point in Figure 2 are calculated using the following formula:

$$\dot{m}_i = \frac{m_{i+1} - m_{i-1}}{(t_{i+1} - t_{i-1})V_{EB}} \tag{33}$$

where $\dot{m}_i$ is the tangent erosion rate for $i^{th}$ point, $m_{i+1}$ and $t_{i+1}$ are eroded mass and time for $(i+1)^{th}$ point, $m_{i-1}$and $t_{i-1}$ are eroded mass and time for $(i-1)^{th}$ point and $V_{EB}$ is the volume of the erosion boundary (i.e., test specimen).

In Eq. (13), $\varphi_0$ is the initial porosity of the test sample before the start of the erosion and $\varphi$ is the porosity of the test sample after the initiation of the erosion process. The difference between these two parameters is computed using the following relationship:

$$\varphi - \varphi_0 = \frac{m}{\rho_s\, V_t} \tag{34}$$

where $m$ is the cumulative mass of eroded solids which is obtained using Eq. (32) and $V_t$ is the total volume of the test specimen (equivalent to $V_{EB}$) . It should be noted that Eq. (34) is a simplified form of Eq. (14).

The diameter of the eroded particles must be smaller than the pore throats which they are moving through. According to the experimental work of Abrams (1977), the particles should have a diameter equal or smaller than one-third of the average pore throat size of the porous medium in order to be able to pass through the pore network without being entrapped. Therefore, the particle diameter $D_p$ used in the calculation of the Reynolds number and critical fluid velocity is assumed to be the harmonic mean diameter of all particles smaller than 1/3 of the average pore throat size of the test specimen. The harmonic mean diameter is calculated using the method suggested by Kovacs (1981).

Different methods are available in the literature to estimate the average pore throat diameter of an assembly of particles based on the grain size distribution curve (e.g., Kovacs, 1981; Uno et al., 1996). The average pore throat size of the test specimen, which is obtained using Figure 1 and the method suggested by Uno et al. (1996), has been computed to be around 14.5 microns. Therefore, $D_p$ is assigned a constant value of 3.7 microns for all tests. As it has been mentioned before, $D_p$ is calculated as the harmonic mean diameter of all particles smaller than 1/3 of average pore throat size. Also, the critical fluid velocity is calculated using Eq. (24) by setting porosity equal to $\varphi_0$ and is assumed to remain constant for all tests. Since the fluid flow is in the upward direction, $\theta_n$ is set to zero in Eq. (25).

Based on the approach discussed above and by using Eq. (12) and Eq. (29), the corresponding values of $\lambda$ and $\omega$ for each test can be obtained from the experimental data (Table 1and Figure 2). Tests 1, 2 and 3 (with hydraulic gradients of 0.18, 0.39 and 0.55, respectively) are used to calibrate the material parameters and Tests 4 and 5 (with hydraulic gradients of 0.60 and 0.75, respectively) are used to validate the proposed model. Figure 3 through Figure 5 show the plots of $ln\,\lambda$ versus $ln\,\omega$ for Tests 1, 2 and 3, respectively.

In Figure 3 through Figure 5, the diamonds represent experimental data and the solid line represents the best linear fit. The corresponding equation for the linear fit is also shown in these plots along with the value of coefficient of determination, $R^2$. Also, in these figures, the upper-right data points correspond to the start of the test and lower-left data points correspond to the end of the test.

As mentioned earlier, in Test 2, a sudden increase in fluid velocity is reported after 5 hours (Sterpi, 2003). Since the value of fluid velocity is used to calculate $\lambda$ and $\omega$ and since the value of velocity after 5 hours is not reported in this test, only data points up to 5 hours after the start of the test are used in calibration of $\alpha$ and $\beta$ (Figure 4).

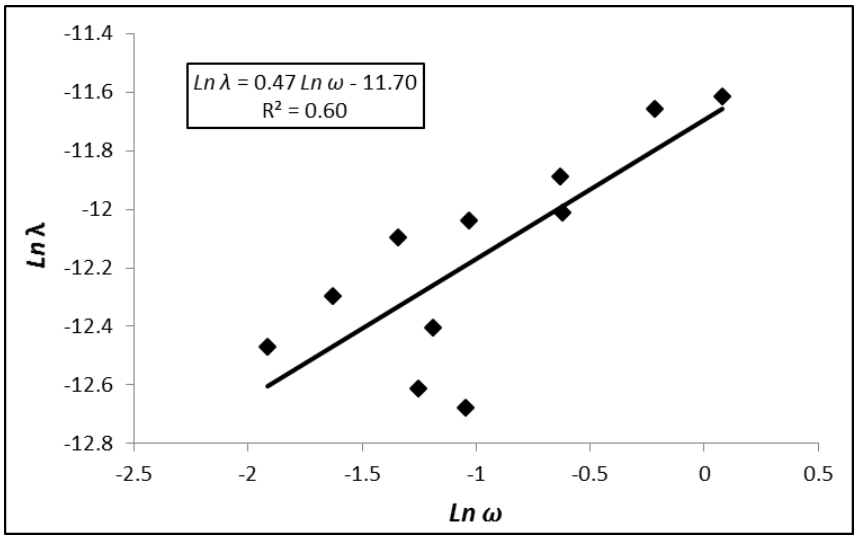


**Figure 3: Calibrating model parameters for Test 1 by Sterpi (2003) (*i=0.18*)**

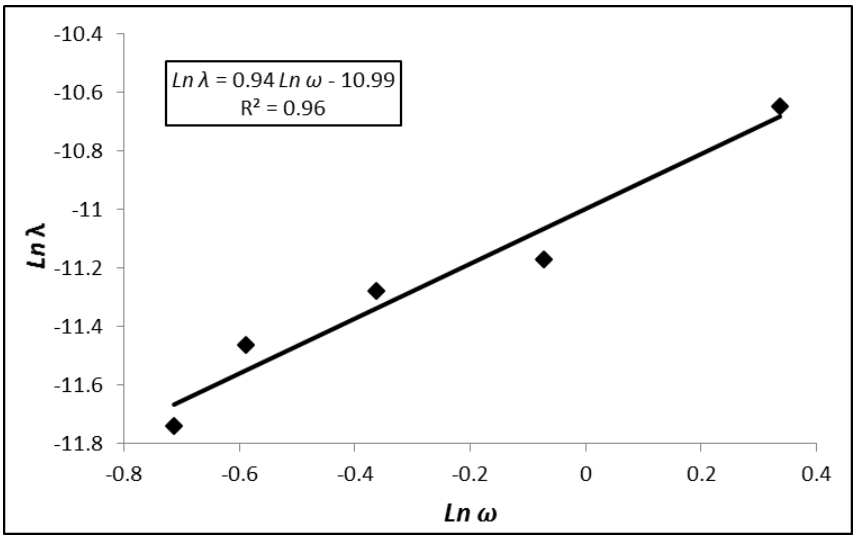


**Figure 4: Calibrating model parameters for Test 2 by Sterpi (2003) (*i=0.39*)**

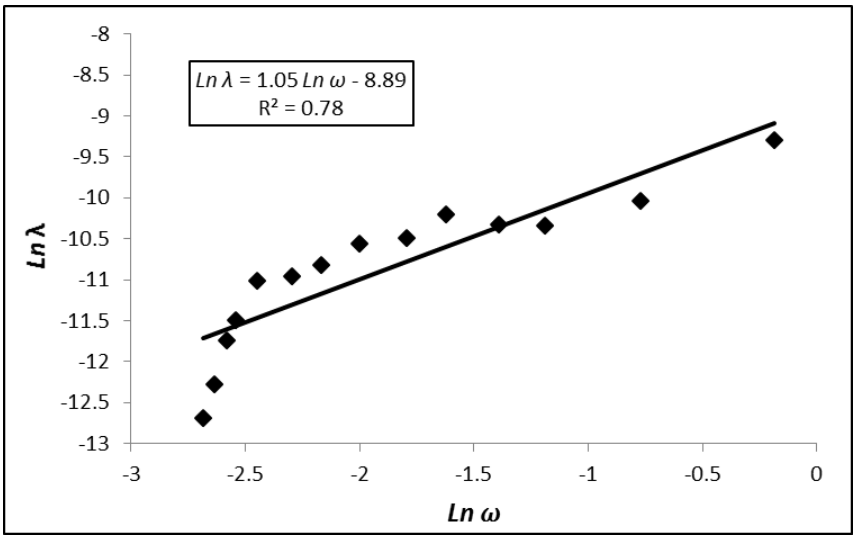


**Figure 5: Calibrating model parameters for Test 3 by Sterpi (2003) (*i=0.55*)**

As observed, the variation of $ln\,\lambda$ versus $ln\,\omega$ for these tests can be approximated using a linear trend. Table 2 shows a summary of calibration parameters for Tests 1, 2 and 3.

**Table 2: Summary of calibration parameters for Tests 1, 2 and 3 performed by Sterpi (2003)**

| Test # | Hydraulic gradient | $\alpha$ | $\beta$ |
|---|---|---|---|
| **1** | 0.18 | 8.29E-6 | 0.47 |
| **2** | 0.39 | 1.69E-5 | 0.94 |
| **3** | 0.55 | 1.38E-4 | 1.05 |

After calibrating the erosion coefficient , $\lambda$, for each test, Eq. (12), Eq. (14) and Eq. (28) are used together to obtain an analytical relationship for the instantaneous (tangent) rate of erosion. With some rearrangement of the abovementioned equations, the following relation is obtained:

$$\frac{\partial \varphi}{\partial t} = \alpha \left[\frac{G_S(Rp - Rp_{cr})}{\varphi - \varphi_0}\right]^{\beta} \frac{(v_f - v_{cr})}{D_p} \tag{35}$$

After integration and simplification of Eq. (35), an analytical relationship for porosity variation, $\varphi - \varphi_0$, is derived in the following form:

$$\varphi - \varphi_0 = \left[\frac{\alpha\,(\beta+1) G_s^{\beta}\,(Re_p - Re_{p,cr})^{\beta}(v_f - v_{cr})\,(t - t_0)}{D_p}\right]^{\frac{1}{(\beta+1)}} \quad \textbf{(36)}$$

By substituting Eq. (36) in Eq. (14), the following relationship is obtained for $\dot{m}$:

$$\dot{m} = K(t - t_0)^{\frac{-\beta}{(\beta+1)}} \quad \textbf{(37)}$$

where $K$ is

$$K = \rho_s \frac{1}{(\beta+1)} \left[\frac{\alpha\,(\beta+1) G_s^{\beta}\,(Re_p - Re_{p,cr})^{\beta}(v_f - v_{cr})}{D_p}\right]^{\frac{1}{(\beta+1)}} \quad \textbf{(38)}$$

As mentioned before, data from Tests 1, 2 and 3 were used for model calibration and a summary of the calibrated parameters for these tests is given in Table 2. Comparisons between the experimental and calculated values of erosion rate for these 3 tests are shown in Figure 6 to Figure 8. In these figures, analytical values of erosion rate are calculated by using Eq. (37) and the data given in Table 1 and Table 2 and the experimental values are calculated using Eq. (33).

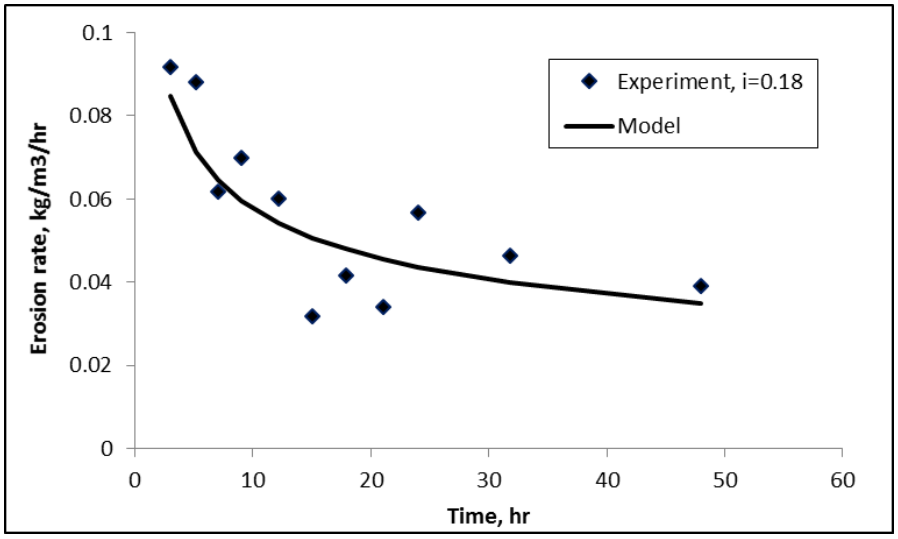


**Figure 6: Comparison between experimental and calculated values of erosion rate, *i=0.18***

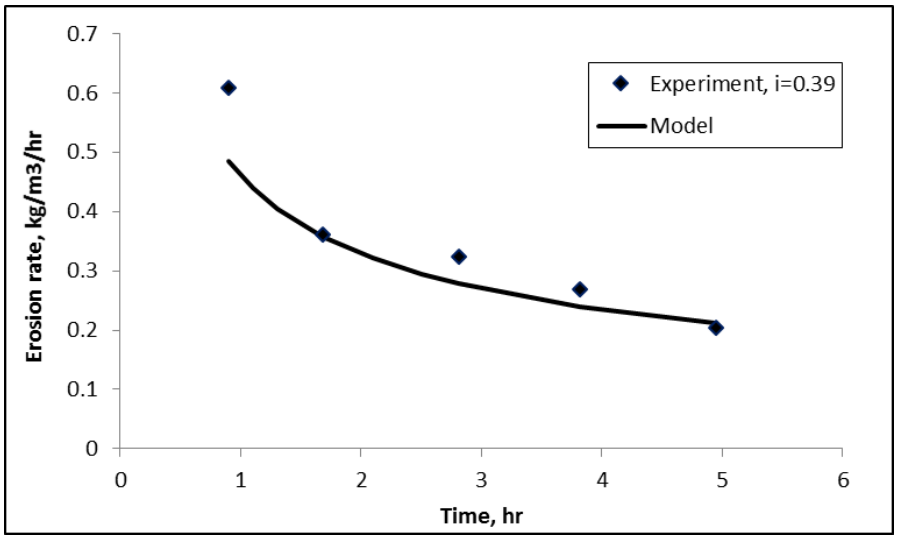


**Figure 7: Comparison between experimental and calculated values of erosion rate, *i=0.39***

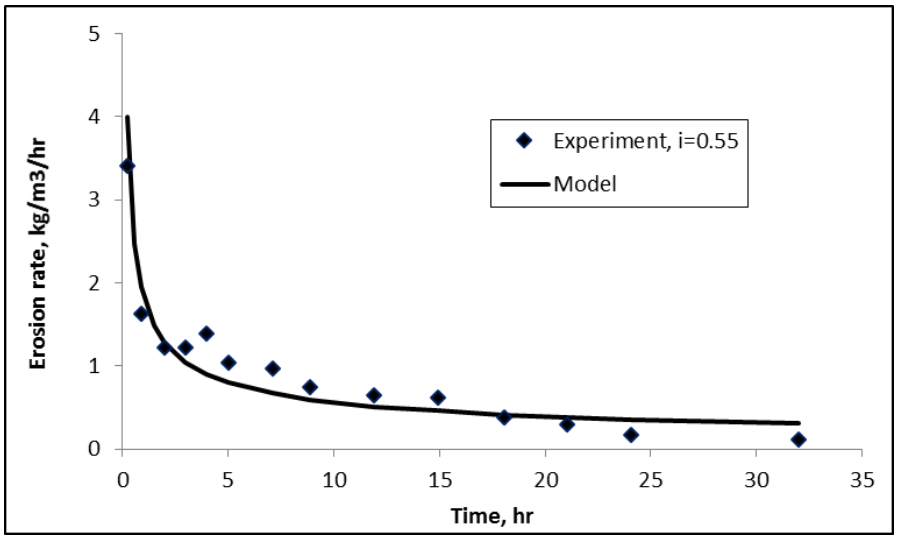


**Figure 8: Comparison between experimental and calculated values of erosion rate, *i=0.55***

## Model Validation

In order to validate the analytical erosion model given in Eq. (37), relationships are required to predict $\alpha$ and $\beta$ for Tests 4 and 5 by just using independent parameters such as hydraulic gradient. The data given in Table 2 are used in order to construct such relationships. Figure 9 and Figure 10 show the variation of $\alpha$ and $\beta$ for Tests 1, 2 and 3 with hydraulic gradient.

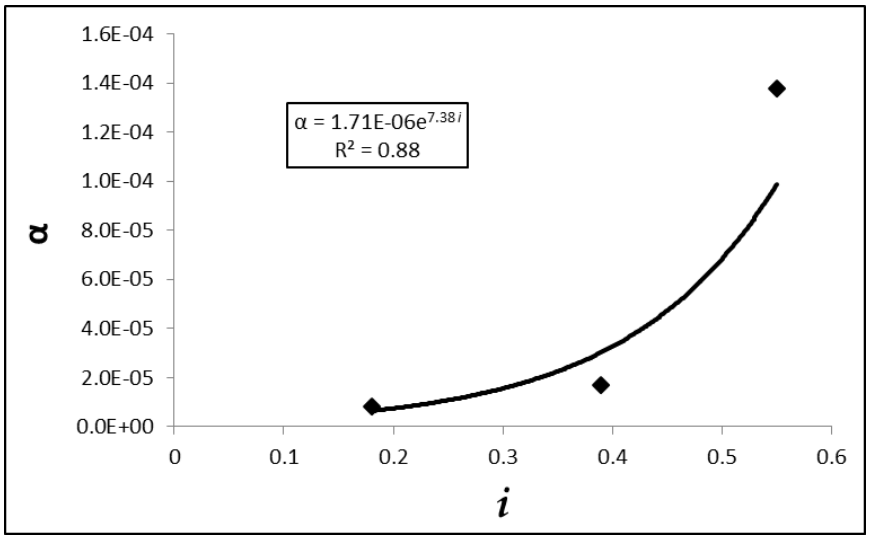


**Figure 9: Variation of $\alpha$ with hydraulic gradient for Tests 1, 2 and 3 and best fit (solid line)**

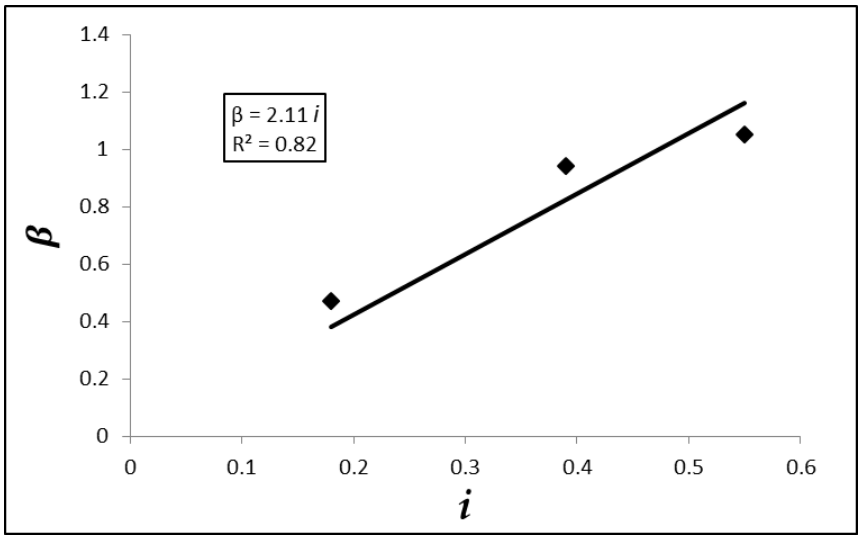


**Figure 10: Variation of $\beta$ with hydraulic gradient for Tests 1, 2 and 3 and best fit (solid line)**

Figure 9 shows that $\alpha$ varies exponentially with hydraulic gradient and Figure 10 suggests that the relationship between $\beta$ and hydraulic gradient is linear. Therefore, based on the trends observed in these figures, the following relationships are suggested for variation of $\alpha$ and $\beta$ with hydraulic gradient.

$$\alpha = \gamma_1 e^{\gamma_2 i} \quad \textbf{(39)}$$

$$\beta = \gamma_3 i \quad \textbf{(40)}$$

In Eq. (39) and Eq. (40), $\gamma_1$, $\gamma_2$ and $\gamma_3$ are model constants which (based on Figure 9 and Figure 10) are calibrated to be 1.71E-6, 7.38 and 2.11 respectively.

The proposed analytical model, which is shown in Eqs. (37) through (40), is validated by using it to predict the experimental results of Tests 4 and 5 (with hydraulic gradients of 0.60 and 0.75, respectively). In the validation process, first, the values of $\alpha$ and $\beta$ for Tests 4 and 5 are calculated by using the calibrated values of $\gamma_1$, $\gamma_2$ and $\gamma_3$ in Eq. (39) and Eq. (40) and by using their corresponding hydraulic gradient. Table 3 shows a summary of calculated values of $\alpha$ and $\beta$ for Tests 4 and 5. In this table, values of $\alpha$ and $\beta$ are obtained by using Eq. (39) and Eq. (40).

**Table 3: Calculated values of $\alpha$ and $\beta$ for Tests 4 and 5**

| Test # | Hydraulic gradient | $\alpha$ | $\beta$ |
|---|---|---|---|
| **4** | 0.60 | 1.43E-4 | 1.27 |
| **5** | 0.75 | 4.33E-4 | 1.58 |

Next, values of erosion rate for these tests are calculated using Eq. (37) and the data given in Table 3. The comparisons between experimental and predicted values of erosion rate for these two tests are presented in Figure 11 and Figure 12. These figures show that the model predictions have a good agreement with the experimental results.

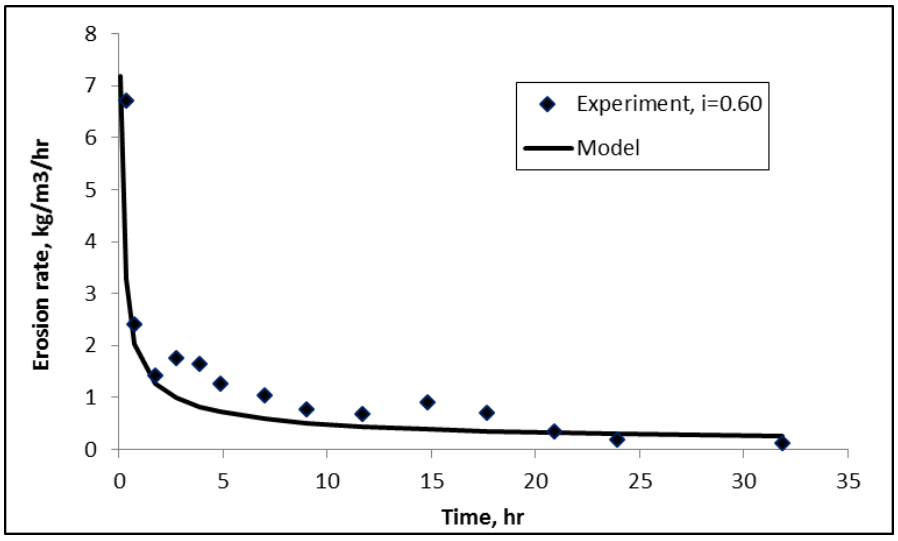


**Figure 11: Comparison between experimental results and model prediction of erosion rate, *i=0.60***

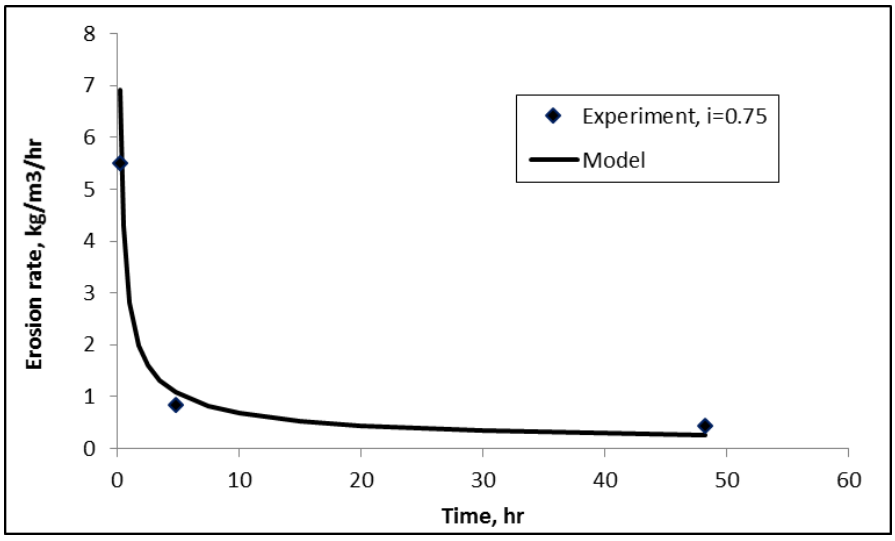


**Figure 12: Comparison between experimental results and model prediction of erosion rate, *i=0.75***

## Discussion and Concluding Remarks

Using the principles of dimensional analysis and approximation theory, an analytical model is proposed to calculate the rate of internal erosion due to fluid flow in a porous medium. The proposed model, shown in Eq. (37) and Eq. (38), shows that the erosion rate has a nonlinear direct relationship with fluid velocity and a nonlinear inverse relationship with time. In other words, for a given hydraulic gradient, erosion rate converges towards zero at a sufficiently large time which is consistent with the physics of erosion process as well as experimental observations. In addition, the higher the hydraulic gradient, the faster the erosion rate decreases with time, which is also consistent with experimental observations. The proposed model has two calibration parameters (Eq. 39-40) which vary as functions of the hydraulic gradient. The model is calibrated and validated using experimental data available in the literature. The validation results show that the model predictions of erosion rates have a good agreement with experimental data.

This model associates vanishing erosion rate to changes in porosity. In other words, for any given hydraulic gradient, there is only a portion of the particle assembly that is erodible. The porosity increases slowly as particles are being washed away to the point where the entire erodible portion has been eroded at which point internal erosion stops. Physically, this can happen due to two reasons. First, at a certain hydraulic gradient, hydrodynamic forces are only able to mobilize particles of a certain size. For a well graded assembly of particles, the lower the hydraulic gradient the smaller the percentage of erodible particles. The second reason for the decreasing internal erosion rate can be related to the processes of particle re-deposition and pore clogging which limit the available flow paths for loose particles to migrate.

Also, it was assumed in this work that the parameter $D_p$, which is the average size of the eroded particles, is constant for all hydraulic gradients. The reason for this assumption is that we do not know the value of $D_p$ *a priori* unless we perform the erosion experiments and analyze the size of eroded particles. The fact of matter is that higher hydraulic gradients mobilize larger size

particles and generally, $D_p$ can vary from one test to another. To further improve this model, a correlation can be established, experimentally, between fluid velocity (or hydraulic gradient) and the average size of the eroded particles. Then, such a correlation can be used to assign variable values for $D_p$ in the proposed erosion model.

The novelty of the analytical model presented in this paper is in its derivation methodology which combines dimensional analysis and approximation theory with the principle of conservation of mass and considers the physics of erosion process as well as experimental and field observations. In addition, this model accounts for the effect of fluid viscosity and average particle diameter on the rate of internal erosion (by using the concept of particle Reynolds number) which are not directly addressed in previously published models. As mentioned earlier, the proposed model has two calibration parameters which are dependent on hydraulic gradient. These parameters are material-dependent and need to be calibrated again in case the porous medium under study is changed.

It should be noted that in this work, the focus was on the development, calibration and validation of an analytical relationship for estimation of the rate of internal erosion. The proposed model can be used in analytical or numerical modelling of internal erosion process in various field phenomena such as fines migration and sand production (petroleum engineering) or suffusion and surface settlement due to internal erosion (geotechnical engineering). It should be noted that this model assumes that internal erosion doesn't bring about any changes in permeability. However, experimental and field observations indicate that internal erosion is generally associated with some degree of permeability reduction in porous media. To apply this model to cases where permeability is reduced as a result of internal erosion, this model has to be coupled with appropriate constitutive laws relating permeability variation to porosity variation or the mass of internally eroded particles.

## Acknowledgments

The authors would like to acknowledge the research funding for this study provided by NSERC through CRDPJ 387606-09.

## Nomenclature

| | |
|---|---|
| A, $B$ | Parameters used to estimate critical fluid velocity |
| $A_{cs}$ | Cross sectional area of an immersed body projected in the direction of flow |
| $c$ | Concentration of solids in fluid phase |
| $c_{cr}$ | Critical concentration of solids in the fluid phase |
| $C_D$ | Drag coefficient |
| $D_p$ | Particle diameter or average particle diameter |
| $F_{D,n}$ | Drag force of fluid exerted on the particle in direction *n* |

| | |
|---|---|
| $F_{G,n}$ | Resistive gravitational force in direction *n* |
| $F_{PG,n}$ | Pressure gradient force exerted on the particle in direction *n* |
| $G_s$ | Specific gravity of the solid particles |
| $i$ | Hydraulic gradient |
| $k$ | Permeability |
| $K$ | Hydraulic conductivity |
| $m$ | Eroded mass |
| $\dot{m}$ | Tangent erosion rate per unit volume |
| $m_t$ | Total mass of the test specimen |
| $n$ | A symbol representing an arbitrary direction |
| $n_p$ | Number of particles |
| $p$ | Percentage of the eroded fine particles |
| $p_{if}$ | Initial percentage of the fine particles |
| $\bar{q}_i$ | Flow flux of the mixture of solids and fluid |
| $Rp$ | Particle Reynolds number |
| $Rp_{cr}$ | Particle Reynolds number calculated at critical fluid velocity |
| $t$ | Time |
| $t_0$ | Time at which erosion starts |
| $v_{A,n}$ | Actual fluid velocity in direction *n* |
| $v_{f,n}$ | Apparent (Darcy) fluid velocity in direction *n* |
| $V_{EB}$ | Volume of the erosion boundary |
| $v_{cr,n}$ | Critical fluid velocity in direction *n* |
| $V_p$ | Volume of particle |
| $V_t$ | Total volume of the sample |
| $\alpha, \beta, \gamma_1, \gamma_2, \gamma_3$ | Dimensionless calibration parameters |
| $\Delta h$ | Hydraulic head difference |
| $\Delta L$ | Sample length |

| | |
|---|---|
| $\theta_n$ | Angle between direction *n* and vertical upward direction |
| $\lambda$ | Erosion coefficient |
| $\mu$ | Fluid dynamic viscosity |
| $\rho_f$ | Fluid density |
| $\rho_s$ | Grain density |
| $\Phi$ | Fluid potential |
| $\varphi$ | Porosity |
| $\varphi_0$ | Original porosity of the assembly of particles |
| $\|\ \ \|$ | Norm of a vector |

## References


Abrams, A., 1977. Mud Design to Minimize Rock Impairment Due to Particle Invasion, JPT, pp. 586-592.

Asgian, M.I., Cundall, P.A., and Brady, B.H.G., 1995. The mechanical stability of propped hydraulic fractures; a numerical study, J. of Pet. Tech., March, pp. 203-208.

Azadbakht, S., Jafarpour, M., Rahmati, H., Nouri, A., Vaziri, H., and Chan, D., 2012. A numerical model for predicting the rate of sand production in injector wells. SPE Deep water and Completions Conference and Exhibition, Galveston, TX, USA, June 20-21.

Baylis J. R., 1937. Experiences in filtration. J. of Amer. Water Works Ass., Vol. 29, pp. 1010-1048.

Bendahmane, F., Marot, D., and Alexis, A., 2008. Experimental Parametric Study of Suffusion and Backward Erosion. J. Geotech. Geoenviron. Eng., Vol. 134, No. 1, pp. 57–67.

Bonelli, S. and Marot, D., 2011. Micromechanical modeling of internal erosion, European Journal of Environmental and Civil Engineering, Vol. 15, No. 8, pp. 1207-1224.

Charlez, Ph. A., 1997. Rock Mechanics: Petroleum Applications. Vol. 2, Editions Technip.

Cividini, A. and Gioda, G., 2004. Finite element approach to the erosion and transport of fine particles in granular soils. Int. J. Geomech., Vol. 4, No 3, pp.191–198.

Cividini, A., Bonomi, S., Vignati, G.C. and Gioda G., 2009. Seepage-induced erosion in granular soil and consequent settlements. Int. J. Geomech., Vol. 9, No. 4, pp. 187–194.

Correia dos Santos, R. N., Caldeira, L. M. M. S., and Maranha das Neves, E., 2015. Laboratory Test for Evaluating Crack Filling During Internal Erosion in Zoned Dams. Geotechnical Testing Journal, Vol. 38, No. 6, pp. 915–928.

David, F. W. and Nolle, H., 1982. Experimental Modelling in Engineering, Butterworths.

de Gaauw, A., Van Der Meulen, T. and Van Der Does De Bye, M., 1984. Design Criteria for Granular Filters, J. Waterway, Port, Coastal, Ocean Eng. Vol. 110, No. 1, pp. 80-96.

Detournay, C. Tan, C., and Wu, B., 2006. Modeling the mechanism and rate of sand production using FLAC, The 4th International FLAC Symposium on Numerical Modeling in Geomechanics, paper: 08-10.

Detournay, C., 2008. Numerical modelling of the slit mode of cavity evolution associated with sand production, SPE Annual Technical Conference, Colorado, USA, September 21-24.

Fjaer, E., Cerasi, P., Li, L., and Papamichos, P., 2004. Modeling the rate of sand production, The 6th North America Rock Mechanics Symposium (NARMS), Houston, TX, USA, June 5–9.

Hornung, H. G., 2006. Dimensional Analysis: Examples of the Use of Symmetry, Dover publications, ISBN: 0486446050

Hunter, R. P., Bowman, E. T., 2018. Visualisation of seepage-induced suffusion and suffosion within internally erodible granular media. Géotechnique, Vol. 68, No. 10, pp. 918-930.

Iwasaki, T., 1937. Some Notes on sand filtration, J. of Amer. Water Works Ass., Vol. 29, No. 10, pp.1591-1602.

Ke, L. and Takahashi, A., 2014. Triaxial Erosion Test for Evaluation of Mechanical Consequences of Internal Erosion. Geotechnical Testing Journal, Vol. 37, No. 2, pp. 1–18.

Kenney, T. C., and Lau, D., 1985. Internal stability of granular filters. Can. Geotech. J., Vol. 22, No. 2, pp. 215–225.

Kovacs, G., 1981. Seepage hydraulics, Elsevier Scientific.

Lafleur, J., 1984. Filter Testing of Broadly Graded Cohesionless Tills. Can. Geotech. J., Vol. 21, pp. 634–643.

Liang Y., Yeh T., Wang J., Liu M., Zha Y. and Hao Y., 2017. An auto-adaptive moving mesh method for the numerical simulation of piping erosion. Computers and Geotechnics, Vol. 82, pp. 237-248.

Muir Wood, D., Maeda, K., and Nukudani, E., 2010. Modelling mechanical consequences of erosion. Géotechnique, Vol. 60, No. 6, pp. 447-457.

Nguyen, V. T., 2012. Flow through filters in embankment dams, PhD thesis, University of Wolongong, Australia.

Papamichos, E., and Malmanger, E.M, 1999. A sand erosion model for volumetric sand predictions in a North Sea reservoir, SPE Latin American and Caribbean Petroleum Engineering Conference, Caracas, Venezuela, 21-23 April.

Papamichos, E., 2010. Erosion and multiphase flow in porous media. Application to sand production, Special issue of Europ. J. of Env. and Civil Eng., Vol. 14/8-9, pp. 1129-1154.

Richards, K. S. and Reddy, K. R., 2010. True Triaxial Piping Test Apparatus for Evaluation of Piping Potential in Earth Structures. Geotech. Test. J., Vol. 33, No. 1, pp. 83–95.

Sakthivadivel, R., 1967. Theory and mechanism of filtration of non-colloidal fines through a porous medium, PhD thesis. University of California, Berkeley

Servant, G., Marchina, P., Peysson, Y., Bemer, E., and Nauroy, J., 2006. Sand erosion in weakly consolidated reservoirs: Experiments and numerical modeling, SPE/DOE Symposium on Improved Oil Recovery, Tulsa, OK, USA, April 22-26.

Skempton, A. W. and Brogan, J. M., 1994. Experiments on piping in sandy gravels, Geotechnique, Vol. 44, No. 3, pp. 449–460.

Skjaerstein, A., Stavropoulou, M., Vardoulakis, I., and Tronvoll, J., 1997. Hydrodynamic erosion; A potential mechanism of sand production in weak sandstones, Int. J. of Rock Mech. and Mining Scien., Vol. 34, No. 3–4, pp. 292.e1-292.e18.

Stavropoulou, M., Papanastasiou, P., and Vardoulakis, I., 1998. Coupled wellbore erosion and stability analysis, Int. J. Numer. Anal. Meth. Geomech., Vol. 22, No. 9, pp. 749-769.

Sterpi, D., 2003. Effects of the erosion and transport of fine particles due to seepage flow. Int. J. Geomech., Vol. 31, pp. 111–122.

Tomlinson, S. S. and Vaid, Y. P., 2000. Seepage Forces and Confining Pressure Effects on Piping Erosion. Can. Geotech. J., Vol. 37, pp. 1–13.

Uno, T., Kamiya, K., Matsushima, T., 1996. The Relationships between Particle Size and Void Diameter for Sand, Proceedings of the Second International Geofilters Conference, pp. 67-74.

Vardoulakis, I., Stavropoulou, M., and Papanastasiou, P., 1996. Hydro-mechanical aspects of the sand production problem, J. of Transp. in Por. Media, Vol. 22, No. 2, pp. 225-244.

Vardoulakis, I., 2006. Sand production, Rev. Europ. de Génie Civil, Vol. 10, No. 6-7, pp. 817-828.

Wang, J., Wan, R. G., Settari, A., and Walters, D., 2005. Prediction of volumetric sand production and wellbore stability analysis of a well at different completion schemes, The 40th U.S. Symposium on Rock Mechanics (USRMS), Anchorage, AK, USA, June 25 – 29.

Wang, Y., and Xue, S., 2002. Coupled reservoir-geomechanics model with sand erosion for sand rate and enhanced production prediction, International Symposium and Exhibition on Formation Damage Control, Lafayette, Louisiana, USA, February 20-21.

Yang J., Yin Z., Laouafa F. and Hicher P., 2018. Internal erosion in dike-on-foundation modeled by a coupled hydromechanical approach, International Journal for Numerical and Analytical Methods in Geomechanics, pp. 1-21.

Yi, X., 2001. Water injectivity decline caused by sand mobilization: Simulation and prediction, SPE Permian Basin Oil and Gas Recovery Conference, Midland, TX, USA, May 15-17.

Zou Y., Chen Q., Chen X. and Cui P., 2013. Discrete numerical modeling of particle transport in granular filters, Computers and Geotechnics, Vol. 47, pp. 48-56.